Programmable Single-Bandpass Photonic RF Filter Based on Kerr Comb from a Microring

Xiaoxiao Xue, Yi Xuan, Hyoung-Jun Kim, Jian Wang, Daniel E. Leaird, Minghao Qi, and Andrew M. Weiner

***Abstract*—Microresonators with a high Kerr nonlinearity show great potential to generate optical frequency combs with ultrabroad spectra, high repetition rate, and high coherence between comb lines. The compact size and possibility of chip-level integration make the Kerr combs attractive for many applications, especially including photonic radiofrequency (RF) filters. In this paper we report the first demonstration of a programmable photonic RF filter based on the Kerr comb from a silicon nitride microring. A novel scheme enabled by the large frequency spacing of the Kerr comb is introduced in order to suppress unwanted RF passbands including the image and periodic passbands. As a result, a single passband is achieved. To the best of our knowledge, this is the first demonstration of a single-bandpass photonic RF filter employing a discrete-wavelength comb source.**

***Index Terms*—Kerr effect, microwave filters, microwave photonics, optical frequency combs, optical resonators.**

I. Introduction

A PHOTONIC radiofrequency (RF) filter is a system which utilizes photonic devices to process electrical RF signals [1]–[3]. The principles are generally classified into two categories: one using optical filters to filter the RF sidebands [4]–[6] and the other based on photonic delay lines [1]–[3], [7]–[11]. In comparison, the optical filter approach has a simpler structure, but the delay line approach is more flexible and thus more common. In the delay line scheme, the RF modulated optical signal is duplicated to many copies (multiple taps) which are time delayed, weight tailored, summed together, and at the end detected by a photodetector to generate the RF output. The low loss and large bandwidth of photonic delay lines is attractive for processing of high-frequency microwave and millimeter-wave signals. Besides, the high flexibility of optical processing gives photonic RF filters several advantages over their electronic counterparts, such as potential for programmable filter shapes, fast tunability, and compatibility with fiber remoting. There are several methods to implement photonic delay lines in photonic RF filters. One of the most promising ways is to use a multiwavelength optical source and dispersion [7]–[11]. In such a scheme, each wavelength is one tap. The tap weights can be easily controlled by manipulating the frequency spacing, phase and power of the wavelengths, making it possible to implement highly programmable photonic RF filters.

The performance of photonic RF filters strongly depends on the number of wavelengths. Larger wavelength number usually means the capability of achieving larger quality factor and larger time-bandwidth product. However, the need for large-wavelength-number optical sources, which might be multiple laser diodes [7], mode-locked lasers [8], or electro-optically generated combs [9], makes the system bulky and of high-cost. Recently, optical frequency comb generation based on the Kerr effect in nonlinear microresonators has shown great potential to reduce the complexity due to compact size and possibility of chip-level integration [12]–[22]. A number of experiments demonstrating generation of frequency combs with desirable qualities, including low noise, high coherence between comb lines, large spectral range, and high repetition rate have been reported [16]–[22]. Many areas will potentially benefit from this novel compact comb generation scheme, especially including photonic RF filtering.

In this paper, we present a detailed investigation of the first demonstration of a programmable photonic RF filter based on an optical Kerr comb from a silicon nitride (SiN) microring resonator [23]. Besides the promising potential for implementing a compact optical frequency comb generator, the ability to realize the Kerr combs with large frequency spacing may also improve the filter performance, as will be demonstrated here. A larger Nyquist zone can be achieved thanks to the increased line spacing of the Kerr combs (hundreds of GHz) compared to those of traditional mode-locked lasers and optoelectronic combs (tens of GHz). Because of the large spectral range (tens to hundreds of nm) of the Kerr combs, a shorter dispersive element is enough to provide the required time aperture. Thus the RF filter latency is reduced. Furthermore, the increased comb line spacing makes it possible to combine optical filtering and RF filtering to suppress unwanted RF passbands. Unwanted RF passbands including image passbands and periodic passbands are well-known drawbacks of photonic RF filters based on discrete multiwavelength optical source [24]. In this paper, we propose a novel structure which can suppress all unwanted passbands and implement a widely tunable and programmable

Manuscript received January 14, 2014; revised February 28, 2014; accepted March 9, 2014. Date of publication March 17, 2014; date of current version September 1, 2014. This work was supported in part by the National Science Foundation under Grant ECCS-1102110, the Air Force Office of Scientific Research under Grant FA9550–12–1–0236, the DARPA PULSE program under Grant W31P40–13–1–0018 from AMRDEC, and by the Office of the Assistant Secretary of Defense for Research and Engineering under the National Security Science and Engineering Faculty Fellowship program under grant N00244–09–1–0068 from the Naval Postgraduate School.

X. Xue, H.-J. Kim, and D. E. Leaird are with the School of Electrical and Computer Engineering, Purdue University, West Lafayette, IN 47907–2035, USA (e-mail: xue40@purdue.edu; sjun27@purdue.edu; leaird@purdue.edu).

Y. Xuan, J. Wang, M. Qi, and A. M. Weiner are also with Birck Nanotechnology Center, Purdue University, West Lafayette, IN 47907, USA and the School of Electrical and Computer Engineering, Purdue University, West Lafayette, IN 47907–2035, USA (e-mail: yxuan@purdue.edu; wang381@purdue.edu; mqi@purdue.edu; amw@purdue.edu).

Color versions of one or more of the figures in this paper are available online at http://ieeexplore.ieee.org.

Digital Object Identifier 10.1109/JLT.2014.2312359

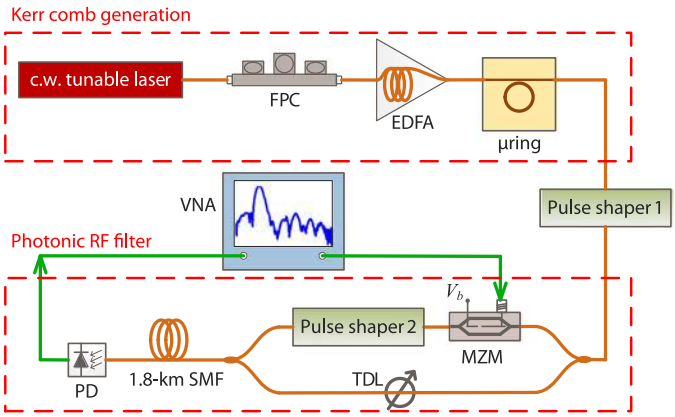

Fig. 1. Experimental setup of broadband Kerr comb generation and photonic RF filter. FPC: fiber polarization controller; EDFA: Erbium-doped fiber amplifier; μ ring: SiN microring; MZM: Mach–Zehnder modulator; TDL: tunable delay line; SMF: single-mode fiber; PD: photodetector; VNA: vector network analyzer.

single passband. To the best of our knowledge, it is the first demonstration of a programmable single-bandpass photonic RF filter utilizing a discrete multiwavelength comb source.

The rest of this paper is organized as follows. Section II shows the experimental setup of the Kerr comb based photonic RF filter. Section III shows broadband Kerr comb generation from a SiN microring. The principle of achieving single passband and the RF filter performance are presented in Section IV. Section V is the conclusion.

II. Setup of the Photonic RF Filter

The experimental setup is shown in Fig. 1. A continuous-wave (c.w.) tunable laser (Agilent 81680A) was used as the pump source for Kerr comb generation. The c.w. light was amplified by a high-power Erbium-doped fiber amplifier and launched into a SiN microring. A polarization controller was used to align the input polarization with the mode which has lower insertion loss and higher quality factor. The Kerr comb generated from the microring was tailored by pulse shaper 1 and launched into the photonic RF filter section. The comb source was split into two branches. One branch was modulated by the RF input signal through a Mach–Zehnder modulator (MZM) and then tailored by pulse shaper 2. The other branch was passed without change except for a small tunable delay, which provides one option for tuning the photonic RF filter passband. The optical signals from the two branches were combined together and went through a 1.8-km single-mode fiber (SMF) which served as a dispersive element. After SMF, a photodetector was used to regenerate the RF output signal. A RF vector network analyzer was used to measure the filter frequency-domain transfer function.

Different from our previous structure of programmable complex-tap photonic RF filter [25], pulse shaper 2 here was moved from the delay branch to the modulation branch. In our previous structure, the tap weights were programmed by controlling the amplitude and phase of the optical carriers. In the novel structure proposed here, a similar function can be performed by controlling the amplitude and phase of the modulation

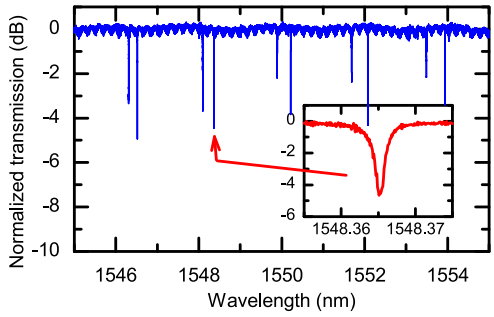

Fig. 2. Transmission of the SiN microring.

sidebands. More importantly, now by programming pulse shaper 2, we can in addition selectively choose and suppress the frequency components of sidebands to suppress unwanted RF passbands. More details will be explained in Section IV.

It is worth noting that the function of pulse shaper 1 is just shaping the Kerr comb spectrum to a more flat shape, so that the tap coefficients can be more easily controlled by pulse shaper 2. In principle, pulse shaper 1 is not needed as long as the extinction ratio of pulse shaper 2 is large enough. In our experiments, the commercial product for pulse shaper2 (Finisar WaveShaper 1000S) has an attenuation control range of 0–35 dB. When the pixels are set to the 'Block' state, the maximum extinction ratio is about 50 dB [26]. For the Kerr comb generated from the microring sample, the power difference between the strongest and the weakest lines in the spectral range concerned (C band) is 28 dB. The tap coefficients are product of the corresponding comb line fields in two arms. Pulse shaper 2 only affects one arm. Without pulse shaper 1, a maximum attenuation of 56 dB is needed by pulse shaper 2 to provide 28 dB attenuation of tap amplitude and make the tap coefficients uniform, which is beyond the extinction ratio limit. Pulse shaper 1 was thus used to flatten the comb spectrum before the comb was launched into the photonic RF filter section.

III. Broadband Kerr Comb Generation

The pump light was coupled into and out of the SiN microring chip through U-grooves and lensed fibers. The radius of the microring is 100 μm. The waveguide width is 2 μm and the height is 550 nm. The transmission is shown in Fig. 2. There are two mode families. The one with higher quality factor was used for comb generation. The free spectral range (FSR) of this mode is 1.85 nm at around 1550 nm. The zoomed-in transmission of the resonance which the pump light was injected into is shown in the inset of Fig. 2. The loaded quality factor is 7×10^5 and the extinction ratio is 4.7 dB.

The insertion loss of the microring chip is about 4 dB. When the pump power was 1.43 W and the wavelength was 1549.3 nm, a broadband comb was generated. Fig. 3 shows the comb spectrum measured by sending $\sim$0.5% of the total power to an optical spectrum analyzer (OSA). It spreads for $\sim$250 nm above the sensitivity of OSA. The line spacing is equal to the 1.85-nm FSR. The power of the pump wavelength is 7 dB higher than those of the $\pm$1st comb lines directly adjacent to the pump wavelength.

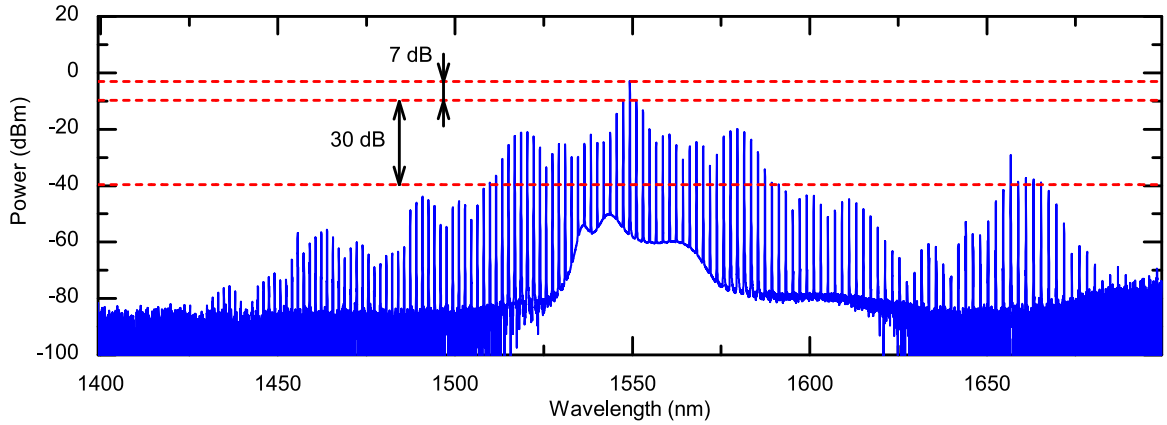

Fig. 3. Spectum of the Kerr comb generated from the microring. (Measured by sending ∼0.5% of the total power to an OSA. The resolution is 0.1 nm.)

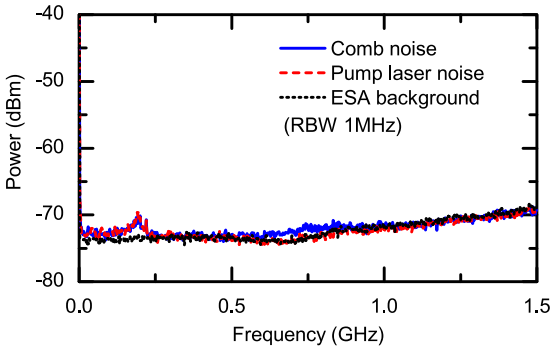

Fig. 4. Intensity noise of all the comb lines.

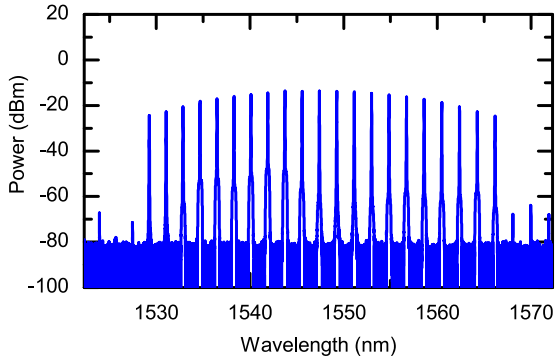

Fig. 5. Shaped comb spectrum after pulse shaper 1.

There are ∼45 lines within 30-dB range relative to the ±1st comb lines. The intensity noise of all the comb lines is shown in Fig. 4. Also shown are the intensity noise of only the pump light and the background noise of the electrical spectrum analyzer. The optical power before photodetector was kept the same for all measurements. The comb shows a very low intensity noise which usually corresponds to high coherence between the comb lines [21], [22].

Twenty-one comb lines in the C band were selected by pulse shaper 1 (the number of comb lines we could select is limited by the spectral range of pulse shaper 1 which is C band), and shaped to be a Hamming window which is a well-known apodization function for suppressing the sidelobes of RF transfer function. The shaped comb spectrum after pulse shaper 1 is shown in Fig. 5. The normalized power of each comb line is given by

$$p_n = 0.54 - 0.46 \times \cos\left[2\pi\left(n + 0.5\right)/N\right] \qquad (1)$$

where $N = 21$ the number of comb lines and $n = 0, 1, \ldots, N-1$ the comb index. To better probe the coherence of the comb lines, the phases were compensated line by line to generate a bandwidth-limited pulse after the pulse shaper 1 [16]. The measured autocorrelation after phase compensation is shown in Fig. 6. Also shown is the calculated ideal plot assuming a stable phase relationship with perfect phase compensation. Excellent agreement is obtained which implies high coherence between the comb lines.

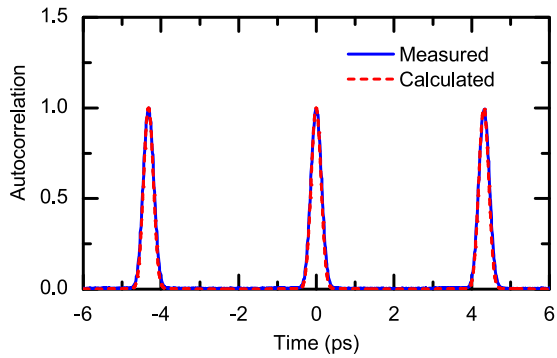

Fig. 6. Autocorrelation of the shaped comb after line-by-line phase compensation by pulse shaper 1.

It is worth noting that although the low noise property is essential, a fixed phase relationship between the comb lines which corresponds to a very high coherence is not necessary for the photonic RF filter we demonstrated here because the optical signals from different taps are detected incoherently. However, in the case of simultaneous frequency conversion and filtering [27], frequency components from different comb lines beat at the photodetector to generate frequency-converted RF signals. High coherence between comb lines is then essential to maintain a low-noise RF output.

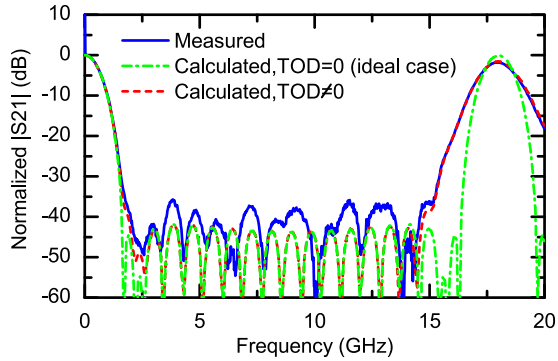

Fig. 7. Baseband RF transfer function.

IV. RF Transfer Functions

A. Baseband Response

First, to calibrate the setup, the RF baseband response was measured. In this measurement, the delay branch was blocked; pulse shaper 2 was programmed to the all-pass state; and the MZM was biased at the quadrature linear point. In this case, the system performs as an all-positive-tap filter, and the RF transfer function shows a baseband response which is low pass in low-frequency region and periodic in high-frequency regions. The dispersion of the SMF is around 30.0 ps/nm giving rise to a tap delay of 55.6 ps. The FSR of RF transfer function is 18 GHz, which is the inverse of the tap delay. The comb spectrum after pulse shaper 1 is as shown in Fig. 5. The theoretical RF transfer function is the Fourier transform of the Hamming window. The measured result is shown in Fig. 7. The measurement agrees with the calculation very well in the baseband. But the high-frequency passband centered at 18 GHz is severely broadened in comparison to the ideal case. This phenomenon is known to be attributed to the third-order dispersion (TOD) [28]–[30]. Nonzero TOD introduces a nonuniform time delay between taps, corresponding to a second-order phase in the tap weights [30]. The theoretical result taking into account the TOD of SMF (which corresponds to a dispersion slope of 0.083 ps/nm^2/km around 1550 nm) is also shown in Fig. 7, and it agrees with the measurement quite well over the full frequency range. For the programmable complex-tap structure as shown in Fig. 1, it has been demonstrated that the TOD induced distortion can be compensated by programming the pulse shaper 2 [30]. More results of TOD compensation are shown in the following subsection.

The measured stopband attenuation is slightly lower than the theoretical value. This is due to the amplitude shaping error of pulse shaper 1. In our experiments, a strategy of feedback and iteration was used to adjust pulse shaper 1. The power deviation of each comb line from the ideal Hamming window is less than ± 0.5 dB.

B. Single-Bandpass RF Filter

When the delay branch is connected and the MZM is biased at the minimum-transmission point, the system performs as a complex-tap RF filter which can be programmed by setting pulse shaper 2. The modulation format is double-sideband

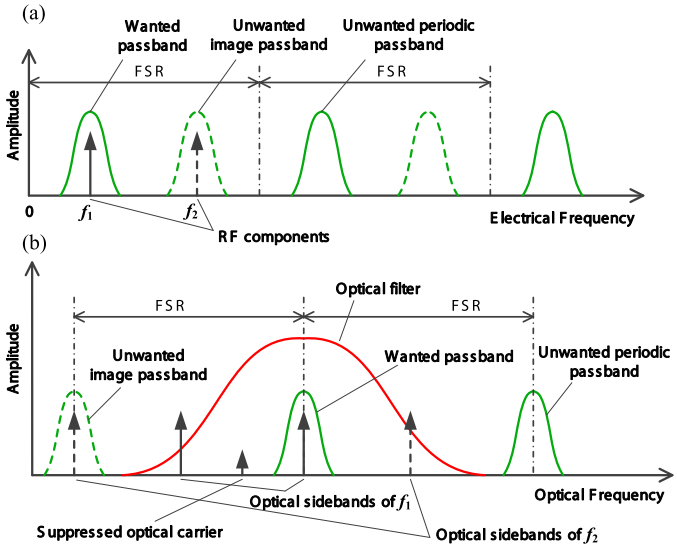

Fig. 8. Illustration of suppressing unwanted RF passbands. (a) Electrical-domain RF transfer function. Two frequency components (f_1 and f_2) are shown; one (f_1) falls in the wanted passband while the other (f_2) falls in the unwanted image passband. (b) Optical-domain transfer function of pulse shaper 2. Only the region around one comb line is shown. The full-range transmission of pulse shaper 2 is a periodic filter with periodicity equal to the comb spacing. The suppressed optical carrier and the optical sidebands corresponding to the RF components f_1 and f_2 are shown. The shapes of the RF passbands are also shown at the corresponding optical sideband positions.

suppressed-carrier (DSB-SC) modulation. In the easiest way, pulse shaper 2 identically controls the upper and lower sidebands to program the tap weights by programming the amplitude and phase in the region around each comb line. The function of this configuration is exactly identical to that of our previous structure for which pulse shaper 2 is placed in the delay branch to control the carriers [25] (supposing the modulation format is also DSB-SC in [25]). The RF transfer function is written as [24]

$$H(\omega_{\mathrm{RF}}) \propto e^{-j\left(\psi_2\omega_{\mathrm{RF}}^2/2+\tau\omega_0\right)} \sum_{n=0}^{N-1} p_n a_n e^{j\phi_n} e^{jn\Delta\omega(\psi_2\omega_{\mathrm{RF}}-\tau)} + e^{j\left(\psi_2\omega_{\mathrm{RF}}^2/2+\tau\omega_0\right)} \sum_{n=0}^{N-1} p_n a_n e^{-j\phi_n} e^{jn\Delta\omega(\psi_2\omega_{\mathrm{RF}}+\tau)} \tag{2}$$

where ψ_2 is the dispersion; τ time delay between the two branches; ω_0 center frequency of comb lines; p_n power of comb lines after pulse shaper 1; a_n and ϕ_n the electric field transmission amplitude and phase of pulse shaper 2 for each tap weight; $\Delta\omega$ the comb line spacing. The two terms in (2) mean two filters with periodic bandpass responses in frequency as illustrated in Fig. 8(a). The FSR of the RF filter response is given by

$$\mathrm{FSR} = 1/(\Delta\omega\psi_2). \tag{3}$$

In practical applications, generally only one filter passband is required which we may call the wanted filter, then the other one is an image filter we do not want. The center frequencies of the wanted filter passband and the unwanted image filter passband

are shifted symmetrically to higher and lower frequencies with respect to integer FSRs by the amount

$$\Delta f = \tau/(2\pi\psi_2). \tag{4}$$

The coexistence of two filters is due to the DSB-SC modulation format employed here. The wanted passband and the unwanted image passband derive from the upper and the lower sidebands respectively. One method of retaining only one filter is to use single-sideband suppressed-carrier (SSB-SC) modulation [9], [25]. A MZM with a more complicated dual parallel structure (DPMZM) is needed. Since there are multiple biases and RF ports, the drift problem is more severe compared to a simple single-electrode MZM. Moreover, the carrier and sideband suppression ratio achieved by a DPMZM is generally not ideal, so a periodic optical filter is needed after the modulator to further improve the suppression ratio.

Here, we demonstrate a novel scheme to eliminate the image filter without the need of SSB-SC modulation. An important change of the system shown in Fig. 1 compared to the previous one [25] is that pulse shaper 2 is moved from the delay branch to the modulation branch after the MZM. By programming pulse shaper 2, we can selectively choose and suppress the frequency components in upper and lower sidebands to suppress unwanted passbands. It is easy to understand this method as achieving SSB-SC modulation by using the amplitude filtering function of pulse shaper 2. We then get the intuitive conclusion that it cannot work when the wanted and unwanted passbands are too close to each other relative to the spectral resolution of pulse shaper 2. The optical spectrum after pulse shaper 2 is indeed quite similar to that of SSB-SC modulation when the two passbands are far away from each other. However, as can be explained in Fig. 8(b), the intrinsic principle of the novel method is to combine optical domain and RF domain filtering functions rather than to implement SSB-SC modulation. In Fig. 8, we suppose the passband from the upper sideband is the one wanted, and the passband from the lower sideband is the image one. Around each comb line frequency, pulse shaper 2 is programmed to be a bandpass filter centered at the optical carrier frequency plus the RF center frequency given by (4). The full-range transmission of pulse shaper 2 is a periodic filter with periodicity equal to the comb spacing. For simplicity, only the region near one comb line is shown in Fig. 8(b). The optical filter bandwidth is larger than the RF filter bandwidth, but smaller than the RF FSR. The sideband components within the optical passband contribute to the wanted RF passband, so the wanted RF passband in the electrical domain is unaffected. However, the sideband components contributing to the image passband are outside the optical filter passband and thus effectively suppressed. One interesting fact is that no matter how close the wanted passband and the unwanted image passband are in the electrical domain, the corresponding sideband components are always separated by one RF FSR in the optical domain. So as long as the bandwidth of the optical filter is much smaller than one RF FSR, the image passband can be effectively suppressed. Another important advantage of this method is that the periodic passbands can also be suppressed simultaneously, making it possible to achieve a real single-bandpass filter.

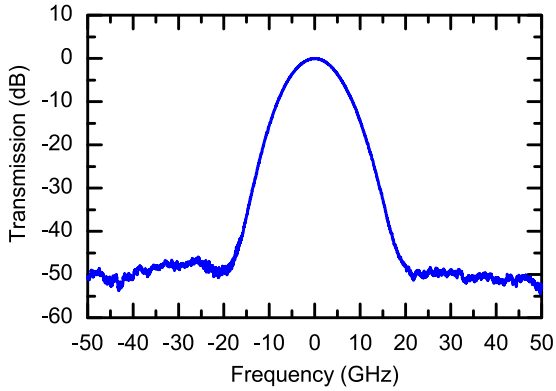

Fig. 9. Normalized transmission of the optical filter implemented by programming pulse shaper 2. The FWHM is 10 GHz. The full-range transmission is periodic at the comb periodicity. Only the region around one comb line is shown here.

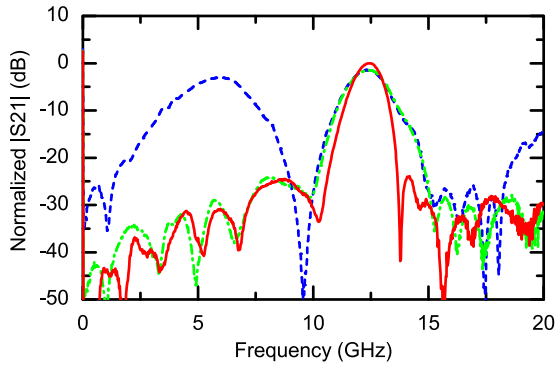

Fig. 10. Measured RF transfer functions in one example of how to achieve a single passband. Dash blue: the unwanted passbands are not suppressed and the distortion not compensated; dash–dot green: the unwanted passbands are suppressed, but the distortion is not compensated; solid red: the unwanted passbands are suppressed and the distortion is compensated.

It is worth noting that the authors of [31] also proposed a complex-tap photonic RF filter employing a pulse shaper to process optical sidebands. But the RF transfer function demonstrated in [31] is not single-bandpass; and the method of implementing complex taps is only proposed for the RF frequencies higher than the resolution of the pulse shaper so that the two optical sidebands and the carrier can be effectively separated by programming the pulse shaper. In comparison, the single-bandpass photonic RF filter we proposed here can work from nearly DC up to almost the whole Nyquist zone. The unique advantage results from the combination of the pulse shaper with the interferometric structure.

In experiments, to prove our idea clearly, the tap delay spacing (thus the length of the SMF) was chosen to give an RF FSR of 18 GHz. The spectral resolution of pulse shaper 2 is 10 GHz. Fig. 9 shows the normalized transmission of pulse shaper 2 when it is programmed to a periodic narrow optical filter with a full-width-at-half-maximum (FWHM) of 10 GHz. All sideband components which are >18 GHz away from the center can be suppressed by more than 45 dB. Fig. 10 shows the measured RF transfer functions in one example of how to achieve a single-bandpass filter. In this measurement, no additional

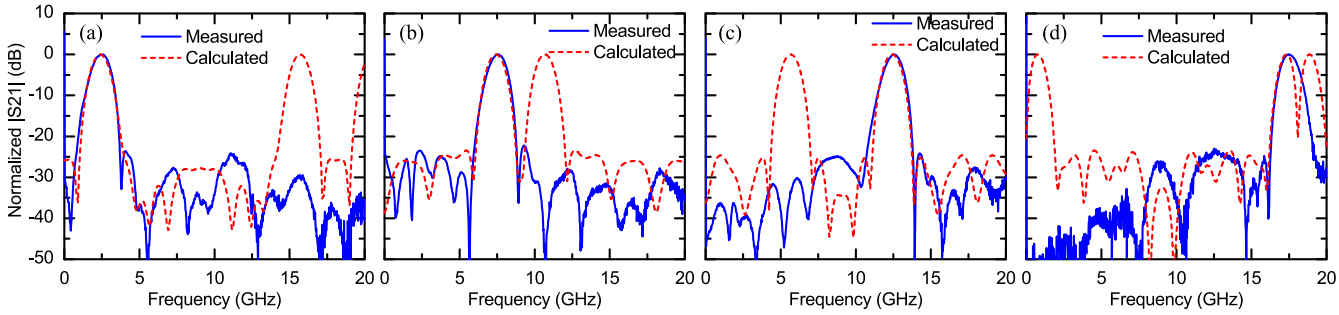

Fig. 11. RF transfer function when the passband is the Fourier transform of a Hamming window and the center frequency is tuned to (a) 2.5 GHz, (b) 7.5 GHz, (c) 12.5 GHz, and (d) 17.5 GHz. The TOD induced RF distortion was compensated in experiments. The calculated results are obtained by considering the comb power ripple of ± 1 dB and assuming pulse shaper 2 is not programmed to suppress the image and periodic passbands.

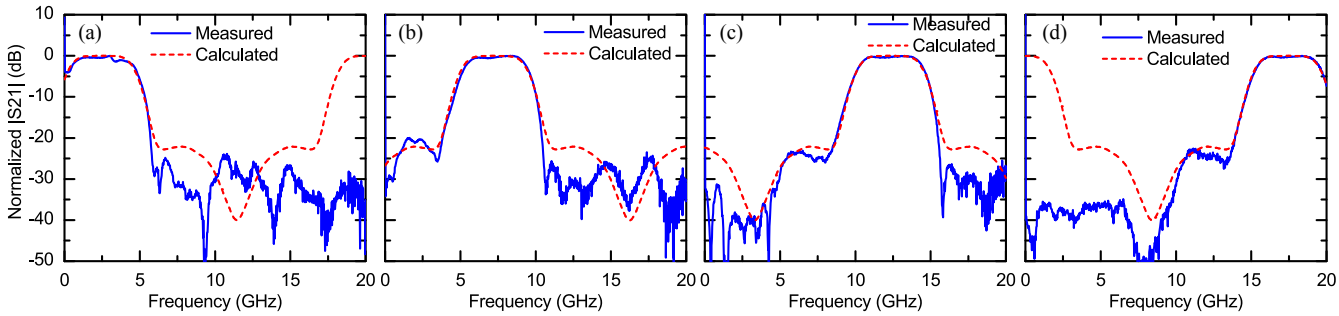

Fig. 12. RF transfer function when the passband is flat-top and the center is tuned to (a) 2.5 GHz, (b) 7.5 GHz, (c) 12.5 GHz, and (d) 17.5 GHz. The TOD induced RF distortion was compensated in experiments. The calculated results are obtained by considering the comb power ripple of ± 1dBand assuming pulse shaper 2 is programmed to suppress the image passbands but not the periodic passbands.

tap weights were applied by pulse shaper 2, so the ideal theoretical RF transfer function is the Fourier transform of the incoming comb shape which is a Hamming window. A linear phase (corresponding to a time delay) was applied to the sidebands by programming pulse shaper 2 to tune the RF passband center [32]. The wanted passband is at about 12.5 GHz, and the image passband at 5.5 GHz. When pulse shaper 2 was programmed to a periodic 10-GHz-wide filter centered at 12.5 GHz higher than the frequency of each comb line, the image passband was eliminated.

It can also be observed in Fig. 10 that the RF passbands are seriously distorted and broadened compared to the theoretical Fourier transform of the Hamming window. This is partially due to the TOD of SMF as mentioned previously. Other causes include the intrinsic dispersion of pulse shaper 2 and the nonuniformity in pixel-to-frequency mapping. These factors induce a phase chirp in the tap weights. Fortunately, by taking advantage of the high programmability of the setup, the distortion can be easily compensated by applying an opposite second-order phase to the tap weights through pulse shaper 2 [30]. The RF transfer function after compensating the distortion is shown in Fig. 10.

C. *Tunability and Programmability*

By changing the time delay between the two branches, the RF passband center can be tuned over a wide range. Experimentally, it is done by programming pulse shaper 2 to change the linear phase slope of the tap weights. Fig. 11 shows the measured single-bandpass RF transfer functions when the RF center was tuned to 2.5 GHz, 7.5 GHz, 12.5 GHz, and 17.5 GHz. The position of the periodic optical filter on pulse shaper 2 which has a setting resolution of 1 GHz [26] was tuned in each case to match the periodic upper sidebands. Fig. 11 also shows the calculated results obtained by assuming the unwanted passbands are not suppressed. The measured and calculated results agree well with each other in the wanted bandpass regions, and all the unwanted passbands are effectively suppressed in the measured results. The FWHM of the retained passband is 1.1 GHz, and the stopband attenuation is $\sim$25 dB. The stopband attenuation gets worse compared to that of the baseband response shown in Fig. 7. It is mainly due to the tap weight error induced by the attenuation error of pulse shaper 2. The tap weight error corresponds to an equivalent comb power ripple of ± 1 dB. The theoretical results shown in Fig. 11 are calculated by taking into account this ripple. The tap weight error can be reduced by improving the attenuation accuracy of pulse shaper 2 and using an iterative strategy to program pulse shaper 2.

One interesting case is how a single passband can be achieved when the RF center frequency is very low so that not all the lower sideband components can be effectively suppressed by pulse shaper 2. In this situation, the optical spectrum after pulse shaper 2 is far from SSB-SC modulation. Actually, it can be understood by noting the fact that the lower sideband components which are not suppressed optically fall in the stopband of the RF image filter; thus suppression in the electrical domain comes into effect here.

By setting pulse shaper 2, the RF transfer function can be arbitrarily programmed. Fig. 12 shows one example of a flat-top

filter. The tap weights are

$$c_n = p_n \cdot \frac{\sin\left[3\pi\left(n+1-n_0\right)/n_0\right]}{3\pi\left(n+1-n_0\right)/n_0} \tag{5}$$

where p_n is given by (1), $n_0 = 11$, and $n = 0, 1, \ldots, N-1$. The FWHM of the RF passband is about 4.3 GHz.

One advantage of electro-optical combs for RF filtering applications is that the timing and repetition rate of the combs can be rapidly controlled to achieve flexible reconfiguration of the RF transfer function, e.g., ultrafast RF passband tuning [9]. One interesting question is whether Kerr combs can be made to such capabilities. Few works in this direction have been done for Kerr combs at this stage. Potential methods that may contribute include external seeding [33], [34] and microresonator tuning [35]. These topics are worthy of future investigation.

D. Nyquist Zone and Filter Latency

For comb-based photonic RF filters, the RF frequency range is limited by half of the comb spacing to avoid sideband mixing from adjacent comb lines. This frequency limit is called a Nyquist zone [32]. The comb spacing of conventional comb sources, such as mode-locked lasers and optoelectronic combs [36], is tens of GHz. So the Nyquist zone is typically limited to a few GHz or at most 10–20 GHz. In comparison, the spacing of the Kerr comb employed here is 231.3 GHz; the corresponding Nyquist zone is as large as 115.6 GHz. The large Nyquist zone is another advantage of Kerr combs for the RF filtering applications.

The RF filter latency demonstrated in this paper is about 9 μs which is due to the latency of the 1.8-km SMF. If we replace the SMF with a dispersion-compensating fiber, which can be significantly shorter for the same dispersion magnitude, the latency can be reduced to $\sim$1 μs. This would be much smaller than those of the filters demonstrated by using optoelectronic comb sources [9], [25], [32]. This is because of the larger spectral range of the Kerr comb which covers the whole C band. The RF bandwidth is proportional to the inverse of the time aperture, which in turn is the dispersion multiplied by the comb spectral range. For a given RF bandwidth, the required dispersion is reduced if the comb spectral range is increased. Thus the length of the dispersion element is reduced, giving rise to reduced filter latency. Microresonators have been demonstrated to be able to generate ultra-wide Kerr combs which spread for tens to hundreds of nm. It is very promising to achieve very low filter latency ($<$1 μs) by using Kerr combs.

It should be pointed out that the filter latency arises from the use of fiber which generally needs a long length to provide the required dispersion amount. If other compact dispersive devices are used, such as chirped fiber Bragg gratings (CFBGs), the filter latency could be further significantly reduced. Kerr combs are not distinguished from electro-optical combs in filter latency for CFBG-based systems, because the grating length does not change significantly with the dispersion as it does for dispersive fibers. However, one issue with CFBGs is the group delay ripple caused by the internal interference effects and system errors in the grating writing process [37], especially when the reflection bandwidth and the dispersion are large. The group delay ripple could be a limitation to achieve a very high RF stopband attenuation which is very sensitive to tap delay ripple.

V. Conclusion

There has been a continuous effort towards chip-level integration of microwave photonic devices and subsystems. Integrated comb generation and shaping is a key technique to implement a compact programmable photonic RF filter and signal processor. For this first demonstration, we used a variety of discrete components and equipment to obtain suitable comb generation from the microring chip. As a result the size and complexity of the overall system remain high in the current experiment. However, if it becomes possible in the future to integrate or package the pump laser, the microring, and possibly a pulse shaper, the complexity and footprint would be greatly reduced. In addition, novel signal processing schemes are made possible because of the large line spacing feature available from Kerr combs. For conventional mode-locked lasers or optoelectronic combs, the line spacing is typically 10–20 GHz. In this case, the resolution of state-of-the-art commercial pulse shapers ($\sim$10 GHz) is not enough to selectively suppress unwanted RF passbands.

Besides the RF transfer function, RF gain, noise figure, and spurious-free dynamic range are also important metrics for evaluating the performances of a photonic RF filter. Another paper submitted to this special issue, based on an electro-optic frequency comb source, focuses on optimizing RF gain and noise figure in a comb-based RF photonic filter [38]. In the current demonstration, we did not concentrate on such performance metrics. The photonic RF filter demonstrated in the current paper has a high RF transmission loss due to low optical power, attributable to a large extent due to the high attenuation necessary in pulse shaper 1 to realize a Kerr comb with smooth shape. To improve the RF gain and reduce the noise figure, an important challenge is generation of Kerr combs with smooth comb spectra and high energy conversion efficiencies. Another possibility would be to try to generate the required comb spectral shape (e.g., a Gaussian shape) directly from the microring, as has been done in the case of electro-optically generated combs [39]. Then no further spectral shaping (thus no corresponding loss) is needed to achieve high RF stopband attenuation.

References

[1] J. Capmany, J. Mora, I. Gasulla, and J. Sancho, "Microwave photonic signal processing," *J. Lightw. Technol.*, vol. 31, no. 4, pp. 571–586, 2013.
[2] J. Capmany, B. Ortega, and D. Pastor, "A tutorial on microwave photonic filters," *J. Lightw. Technol.*, vol. 24, no. 1, pp. 201–229, 2006.
[3] R. A. Minasian, "Photonic signal processing of microwave signals," *IEEE Trans. Microw. Theory Tech.*, vol. 54, no. 2, pp. 832–846, Feb. 2006.
[4] J. Palací, G. Eduardo, V. Jose, V. Galán, J. Martí, and B. Vidal, "Single bandpass photonic microwave filter based on a notch ring resonator," *IEEE Photon. Technol. Lett.*, vol. 22, no. 17, pp. 1276–1278, Sep. 2010.
[5] J. Palací, P. Pérez-Millán, G. E. Villanueva, J. L. Cruz, M. V. Andrés, J. Martí, and B. Vidal, "Tunable photonic microwave filter with single bandpass based on a phase-shifted fiber Bragg grating," *IEEE Photon. Technol. Lett.*, vol. 22, no. 19, pp. 1467–1469, Oct. 2010.
[6] W. Zhang and R. A. Minasian, "Widely tunable single-passband microwave photonic filter based on stimulated Brillouin scattering," *IEEE Photon. Technol. Lett.*, vol. 23, no. 23, pp. 1775–1777, Dec. 2011.

[7] J. Capmany, D. Pastor, and B. Ortega, "New and flexible fiber-optic delay-line filters using chirped Bragg gratings and laser arrays," *IEEE Trans. Microw. Theory Tech.*, vol. 47, no. 7, pp. 1321–1326, Jul. 1999.
[8] A. Ortigosa-Blanch, J. Mora, J. Capmany, B. Ortega, and D. Pastor, "Tunable radio-frequency photonic filter based on an actively mode-locked fiber laser," *Opt. Lett.*, vol. 31, no. 6, pp. 709–711, 2006.
[9] V. R. Supradeepa, C. M. Long, R. Wu, F. Ferdous, E. Hamidi, D. E. Leaird, and A. M. Weiner, "Comb-based radiofrequency photonic filters with rapid tunability and high selectivity," *Nature Photon.*, vol. 6, pp. 186–194, 2012.
[10] X. Xue, X. Zheng, H. Zhang, and B. Zhou, "Highly reconfigurable microwave photonic single-bandpass filter with complex continuous-time impulse responses," *Opt. Exp.*, vol. 20, no. 24, pp. 26929–26934, 2012.
[11] L. Li, X. Yi, T. X. H. Huang, and R. A. Minasian, "Distortion-free spectrum sliced microwave photonic signal processor: Analysis, design and implementation," *Opt. Exp*, vol. 20, no. 10, pp. 11517–11528, 2012.
[12] P. Del'Haye, A. Schliesser, O. Arcizet, T. Wilken, R. Holzwarth, and T. J. Kippenberg, "Optical frequency comb generation from a monolithic microresonator," *Nature*, vol. 450, pp. 1214–1217, 2007.
[13] J. S. Levy, A. Gondarenko, M. A. Foster, A. C. Turner-Foster, A. L. Gaeta, and M. Lipson, "CMOS-compatible multiple-wavelength oscillator for on-chip optical interconnects," *Nature Photon.*, vol. 4, pp. 37–40, 2010.
[14] L. Razzari, D. Duchesne, M. Ferrera, R. Morandotti, S. Chu, B. E. Little, and D. J. Moss, "CMOS-compatible integrated optical hyperparametric oscillator," *Nature Photon.*, vol. 4, pp. 41–45, 2010.
[15] T. J. Kippenberg, R. Holzwarth, and S. A. Diddams, "Microresonator-based optical frequency combs," *Science*, vol. 332, pp. 555–559, 2011.
[16] F. Ferdous, H. Miao, D. E. Leaird, K. Srinivasan, J. Wang, L. Chen, L. T. Varghese, and A. M. Weiner, "Spectral line-by-line pulse shaping of on-chip microresonator frequency combs," *Nature Photon.*, vol. 5, pp. 770–776, 2011.
[17] S. Saha, Y. Okawachi, B. Shim, J. S. Levy, R. Salem, A. R. Johnson, M. A. Foster, M. R. E. Lamont, M. Lipson, and A. L. Gaeta, "Modelocking and femtosecond pulse generation in chip-based frequency combs," *Opt. Exp.*, vol. 21, no. 1, pp. 1335–1343, 2013.
[18] T. Herr, V. Brasch, J. D. Jost, C. Y. Wang, N. M. Kondratiev, M. L. Gorodetsky, and T. J. Kippenberg, "Temporal solitons in optical microresonators," *Nature Photon.*, vol. 8, pp. 145–152, 2014.
[19] P. Del'Haye, S. B. Papp, and S. A. Diddams, "Self-injection locking and phase-locked states in microresonator-based optical frequency combs," *Phys. Rev. Lett.*, vol. 112, 043905, 2014.
[20] S. Papp, P. Del'Haye, and S. Diddams, "Parametric seeding of a microresonator optical frequency comb," *Opt. Exp.*, vol. 21, no. 15, pp. 17615–17624, 2013.
[21] T. Herr, K. Hartinger, J. Riemensberger, C. Y. Wang, E. Gavartin, R. Holzwarth, M. L. Gorodetsky, and T. J. Kippenberg, "Universal formation dynamics and noise of Kerr-frequency combs in microresonators," *Nature Photon.*, vol. 6, pp. 480–487, 2012.
[22] P.-H. Wang, F. Ferdous, H. Miao, J. Wang, D. Leaird, K. Srinivasan, L. Chen, V. Aksyuk, and A. M. Weiner, "Observation of correlation between route to formation, coherence, noise, and communication performance of Kerr combs," *Opt. Exp.*, vol. 20, no. 28, pp. 29284–29295, 2012.
[23] X. Xue, H.-J. Kim, Y. Xuan, J. Wang, D. E. Leaird, M. Qi, and A. M. Weiner, "First demonstration of a tunable single-bandpass photonic radiofrequency filter based on optical frequency comb from a microring," presented at the Opt. Fiber Commun. Conf., San Francisco, CA, USA, 9–13, Mar. 2014.
[24] E. Hamidi, R. Wu, V. R. Supradeepa, C. M. Long, D. E. Leaird, and A. M. Weiner, "Tunable radio frequency photonic filter based on intensity modulation of optical combs," in *Proc. IEEE Topical Meeting Microw. Photon.*, Oct. 2010, pp. 393–396.
[25] M. Song, C. M. Long, R. Wu, D. Seo, D. E. Leaird, and A. M. Weiner, "Reconfigurable and tunable flat-top microwave photonic filters utilizing optical frequency combs," *IEEE Photon. Technol. Lett.*, vol. 23, no. 21, pp. 1618–1620, Nov. 2011.
[26] Finisar Corporation, WaveShaper User Manual, Revision G, Sunnyvale, CA, USA, 2013, pp. 79.
[27] V. Torres-Company, D. E. Leaird, and A. M. Weiner, "Simultaneous broadband microwave downconversion and programmable complex filtering by optical frequency comb shaping," *Opt. Lett.*, vol. 37, no. 19, pp. 3993–3995, 2012.
[28] J. Mora, B. Ortega, A. Díez, J. L. Cruz, M. V. Andrés, J. Capmany, and D. Pastor, "Photonic microwave tunable single-bandpass filter based on a Mach–Zehnder interferometer," *J. Lightw. Technol.*, vol. 24, no. 7, pp. 2500–2509, 2006.
[29] X. Yi, T. X. H. Huang, L. Li, and R. A. Minasian, "Overcoming tap-delay-variation induced distortion in microwave photonic filters," *IEEE Photon. Technol. Lett.*, vol. 24, no. 8, pp. 691–693, Apr. 2012.
[30] X. Xue, X. Zheng, H. Zhang, and B. Zhou, "Analysis and compensation of third-order dispersion induced RF distortions in highly reconfigurable microwave photonic filters," *J. Lightw. Technol.*, vol. 31, no. 13, pp. 2263–2270, 2013.
[31] X. Yi, T. X. H. Huang, and R. A. Minasian, "Tunable and reconfigurable photonic signal processor with programmable all-optical complex coefficients," *IEEE Trans. Microw. Theory Tech.*, vol. 58, no. 11, pp. 3088–3093, Nov. 2010.
[32] E. Hamidi, D. E. Leaird, and A. M. Weiner, "Tunable programmable microwave photonic filters based on an optical frequency comb," *IEEE Trans. Microw. Theory Tech.*, vol. 58, no. 11, pp. 3269–3278, Nov. 2010.
[33] S. Papp, P. Del'Haye, and S. Diddams, "Parametric seeding of a microresonator optical frequency comb," *Opt. Exp.*, vol. 21, no. 15, pp. 17615–17624, 2013.
[34] Y. Liu, Y. Xuan, P. Wang, D. Leaird, L. Fan, L. Varghese, M. Qi, and A. Weiner, "Dual-pump generation of on-chip combs with low intensity noise," in Proceedings. of Frontiers in Optics 2013, I. Kang, D. Reitze, N. Alic, and D. Hagan, Eds., Washington, DC, USA: OSA Technical Digest (online) (Optical Society of America, 2013, paper FM4E.3.
[35] X. Xue, Y. Xuan, P. H. Wang, J. Wang, D. E. Leaird, M. Qi, and A. M. Weiner, "Tunable Frequency Comb Generation from a Microring with a Thermal Heater," to be presented on *Conf. Lasers Electro-opt.*, 2014, arXiv:1402.5438.
[36] V. Torres-Company and A. M. Weiner, "Optical frequency comb technology for ultra-broadband radio-frequency photonics," to appear in *Laser Photon. Rev.*, 2014. arXiv:1403.2776.
[37] R. Kashyap, "Chapter 7: Chirped Fiber Bragg Gratings," in *Fiber Bragg Gratings*. New York, NY, USA: Elsevier Inc, 2009, pp. 306–319.
[38] H.-J. Kim, D. E. Leaird, A. J. Metcalf, and A. M. Weiner, "Comb-Based RF photonic filters based on interferometric configuration and balanced detection," submitted to *J. Lightw.,* Technol.
[39] R. Wu, C. M. Long, D. E. Learid, and A. M. Weiner, "Directly generated Gaussian-shaped optical frequency comb for microwave photonic filtering and picosecond pulse generation," *IEEE Photon. Technol. Lett.*, vol. 24, no. 17, pp. 1484–1486, Sep. 2012.

Xiaoxiao Xue received the B.S. and Ph.D. degrees in electronic engineering with the highest honors from Tsinghua University, Beijing, China, in 2007 and 2012, respectively. Since 2013, he has been working as a Postdoctoral Researcher in the Ultrafast Optics and Optical Fiber Communications Laboratory, Purdue University, West Lafayette, IN, USA. His research interests include microresonator-based Kerr comb generation, microwave photonic signal processing, radio over fiber, and phased array antennas. Dr. Xue was a recipient of the 2012 Wang Daheng Prize funded by the Optical Society of China for his Ph.D. dissertation on microwave photonic signal processing.

Yi Xuan received the B.S. and M.S. degrees in chemistry from the East China University of Science and Technology, Shanghai, China, in 1994 and 1997, respectively, and the Ph.D. degree in inorganic materials from the Tokyo Institute of Technology, Tokyo, Japan, in 2001. Between 2001 and 2005, he was a Postdoctoral Researcher with the National Institute for Materials Science and the National Institute of Advanced Industrial Science and Technology, Tsukuba, Japan. Since August 2005, he has been a Researcher with the School of Electrical and Computer Engineering, Purdue University, West Lafayette, IN, USA, where he is involved in research on nano-CMOS and photonics.

Hyoung-Jun Kim received the B.S. degree in electrical engineering from Kwangwoon University, Seoul, South Korea, in 2005. He received the M.S. and Ph.D. degrees in electrical engineering from Gwangju Institute of Science and Technology (GIST), Gwangju, South Korea, in 2007 and 2011, respectively. From 2011 to 2012, he was at the High Speed Integrated Circuit Laboratory, GIST, where he engaged in research on millimeter-wave communication systems utilizing RF photonics technologies. In 2012, he joined the Ultrafast Optics group in Purdue University, West Lafayette, IN, USA, where he is currently working on reconfigurable RF photonic filters based on optical frequency combs and optical pulse shaping.

Jian Wang received the B.S. degree in optical engineering with the highest honor from Zhejiang University, Hangzhou, China, in 2006. Since 2008, he has been working toward the Ph.D. degree in the School of Electrical and Computer Engineering, Purdue University West Lafayette, IN, USA. His research interests include photonic crystals, silicon photonics, nonlinear optics, and microwave photonics. He has authored and coauthored more than 40 journal articles and conference papers. He has served as a Reviewer for *Optics Letters*, *Optics Express*, *Optics Communication*, and *Nature Scientific Reports*.

Daniel E. Leaird was born in Muncie, IN, USA, in 1964. He received the B.S. degree in physics from Ball State University, Muncie, in 1987, and the M.S. and Ph.D. degrees from the School of Electrical and Computer Engineering, Purdue University, West Lafayette, IN, in 1996 and 2000, respectively. He joined Bellcore as a Senior Staff Technologist in 1987, and later advanced to Member of Technical Staff. From 1987 to 1994, he worked in the Ultrafast Optics and Optical Signal Processing Research Group, where he was a key team member in research projects in ultrafast optics, such as optical pulse shaping using liquid-crystal modulator arrays, investigation of dark soliton propagation in optical fibers, impulsive stimulated Raman scattering in molecular crystals, and all-optical switching. Since 1994, he has been a Senior Research Scientist and Laboratory Manager of the Ultrafast Optics and Optical Fiber Communications Laboratory, the School of Electrical and Computer Engineering, Purdue University. He has coauthored approximately 90 journal articles and 120 conference proceedings and has three issued U.S. patents. He is active in the optics community and professional organizations, including the Optical Society of America and the IEEE Photonics Society, where he served as the Chair of the Ultrafast Optics Technical Committee from 2006 to 2009. He has also served a Consultant to venture capitalists by performing technical due diligence. He also serves as a frequent Reviewer for *Optics Letters*, *Photonics Technology Letters*, *Applied Optics*, and the *Journal of the Optical Society of America B*, in addition to serving on the National Science Foundation review panels in the SBIR program. Dr. Leaird has received several awards for his work in the ultrafast optics field, including a Bellcore Award of Excellence, a Magoon Award for outstanding teaching, and an Optical Society of America/New Focus Student Award.

Minghao Qi received the B.S. degree from the University of Science and Technology of China, Anhui, China, and the M.S. and Ph.D. degrees in electrical engineering from the Massachusetts Institute of Technology, Cambridge, MA, USA, in 2005. In 2005, he joined Purdue University, West Lafayette, IN, USA, where he is currently leading the Photonics and Nano-Fabrication Lab, School of Electrical and Computer Engineering. He is also with the Shanghai Institute of Microsystem and Information Technology, Chinese Academy of Sciences, Shanghai, China.

Andrew M. Weiner graduated from Massachusetts Institute of Technology, Cambridge, MA, USA, with an Sc.D. degree in electrical engineering, in 1984. Upon graduation he joined Bellcore, first as a Technical Staff Member and later as a Manager of Ultrafast Optics and Optical Signal Processing Research. He moved to Purdue University West Lafayette, IN, USA, in 1992, and is currently the Scifres Family Distinguished Professor of electrical and computer engineering. His research interests include ultrafast optics signal processing and applications to high-speed optical communications and ultrawideband wireless. He is especially well known for his pioneering work on programmable femtosecond pulse shaping using liquid crystal modulator arrays. He is the author of a textbook entitled *Ultrafast Optics* (New York, NY, USA: Wiley) and has published more than 250 journal articles. He is a Fellow of the OSA and a Member of the U.S. National Academy of Engineering. He has served as the Chair or Co-Chair of the Conference on Lasers and Electro-Optics, the International Conference on Ultrafast Phenomena, and the National Academy of Engineering's Frontiers of Engineering symposium, as the Secretary/Treasurer of the IEEE Lasers and Electro-Optics Society, and as the Vice-President of the International Commission on Optics. He is currently the Editor-in-chief of *Optics Express*. Dr. Weiner has won numerous awards for his research, including the Hertz Foundation Doctoral Thesis Prize, the OSA Adolph Lomb Medal, the ASEE Curtis McGraw Research Award, the International Commission on Optics Prize, the IEEE LEOS William Streifer Scientific Achievement Award, the Alexander von Humboldt Foundation Research Award for Senior U.S. Scientists, the OSA R.W. Wood Prize, and the IEEE Photonics Society Quantum Electronics Award.